AD-A155059

AD-A155 059

CRREL REPORT 85-8

US Army Corps of Engineers
Cold Regions Research & Engineering Laboratory

Ice fog as an electro-optical obscurant

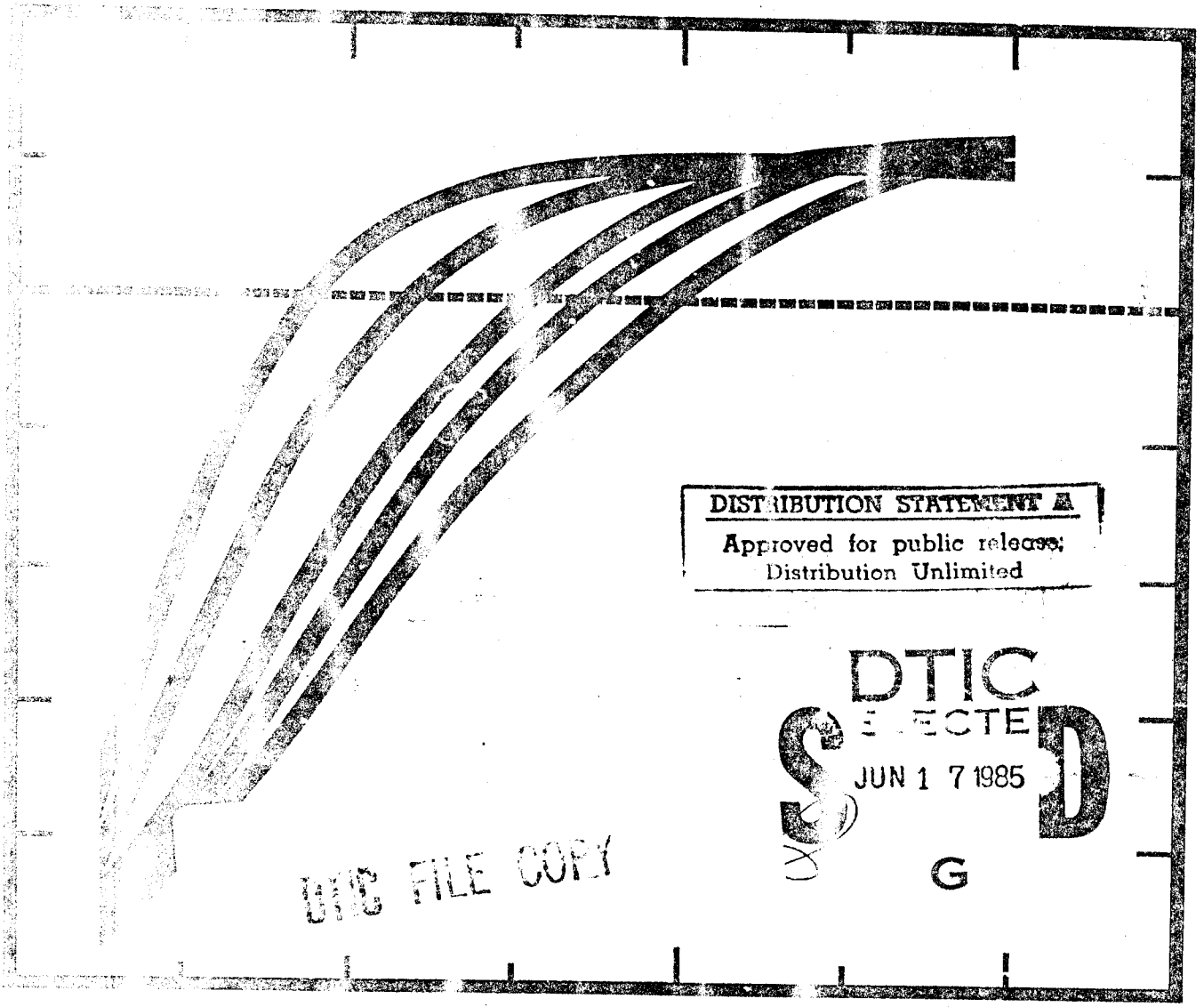

DISTRIBUTION STATEMENT A
Approved for public release;
Distribution Unlimited

DTIC
ELECTE
JUN 17 1985
S
D
G

DTIC FILE COPY

85 5 20 037

DISCLAIMER NOTICE

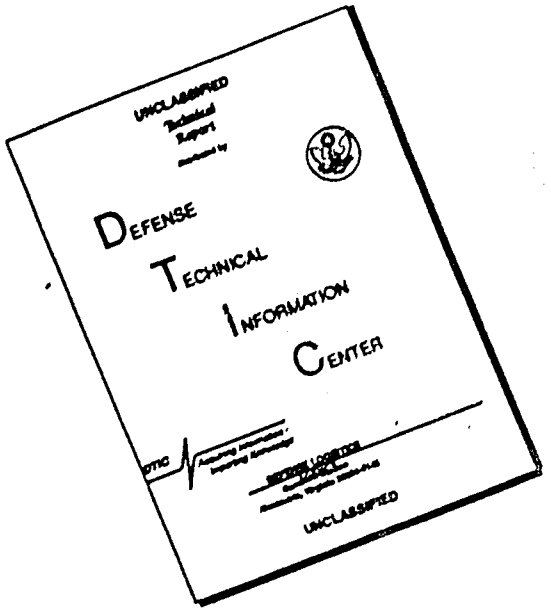

THIS DOCUMENT IS BEST QUALITY AVAILABLE. THE COPY FURNISHED TO DTIC CONTAINED A SIGNIFICANT NUMBER OF PAGES WHICH DO NOT REPRODUCE LEGIBLY.

For conversion of SI metric units to U.S./British customary units of measurement consult ASTM Standard E380, Metric Practice Guide, *published by the American Society for Testing and Materials, 1916 Race St., Philadelphia, Pa. 19103.*

Cover: See Figure 7.

CRREL Report 85-8

March 1985

Ice fog as an electro-optical obscurant

Gary Koh

Accession For	
NTIS GRA&I	☒
DTIC TAB	☐
Unannounced	☐
Justification	
By	
Distribution/	
Availability Codes	
Dist	Avail and/or Special
A/1	

DTIC COPY

Prepared for
OFFICE OF THE CHIEF OF ENGINEERS
Approved for public release; distribution is unlimited.

Unclassified

SECURITY CLASSIFICATION OF THIS PAGE *(When Data Entered)*

REPORT DOCUMENTATION PAGE

READ INSTRUCTIONS BEFORE COMPLETING FORM

1. REPORT NUMBER: CRREL Report 85-8	2. GOVT ACCESSION NO.
3. RECIPIENT'S CATALOG NUMBER	
4. TITLE *(and Subtitle)*: ICE FOG AS AN ELECTRO-OPTICAL OBSCURANT	5. TYPE OF REPORT & PERIOD COVERED
	6. PERFORMING ORG. REPORT NUMBER
7. AUTHOR(s): Gary Koh	8. CONTRACT OR GRANT NUMBER(s)
9. PERFORMING ORGANIZATION NAME AND ADDRESS: U.S. Army Cold Regions Research and Engineering Laboratory, Hanover, New Hampshire 03755-1290	10. PROGRAM ELEMENT, PROJECT, TASK AREA & WORK UNIT NUMBERS: DA Task 4A161102AT24, Task A, Work Unit 004
11. CONTROLLING OFFICE NAME AND ADDRESS: Office of the Chief of Engineers, Washington, D.C. 20314	12. REPORT DATE: March 1985
	13. NUMBER OF PAGES: 18
14. MONITORING AGENCY NAME & ADDRESS *(if different from Controlling Office)*	15. SECURITY CLASS. *(of this report)*: Unclassified
	15a. DECLASSIFICATION/DOWNGRADING SCHEDULE

16. DISTRIBUTION STATEMENT *(of this Report)*

Approved for public release; distribution is unlimited.

17. DISTRIBUTION STATEMENT *(of the abstract entered in Block 20, if different from Report)*

18. SUPPLEMENTARY NOTES

19. KEY WORDS *(Continue on reverse side if necessary and identify by block number)*

Electromagnetic radiation
Ice fog
Obscuration

20. ABSTRACT *(Continue on reverse side if necessary and identify by block number)*

The extinction of visible light and infrared radiation (at wavelengths of 3.5 and 10.6 μm) by ice fog is considered utilizing theoretical concepts and historical experimental data. The reliability of the spherical approximation of ice fog for Mie calculations is examined and judged adequate for forward scatter situations but limited for side and backscatter applications. The relative efficacy in penetrating ice fog as a function of size distribution is evaluated for the wavelengths considered.

DD FORM 1 JAN 73 1473 EDITION OF 1 NOV 65 IS OBSOLETE

Unclassified

SECURITY CLASSIFICATION OF THIS PAGE *(When Data Entered)*

PREFACE

This report was prepared by Gary Koh, Physical Scientist, Geophysical Sciences Branch, Research Division, U.S. Army Cold Regions Research and Engineering Laboratory. Funding for this research was provided by DA Project 4A161102AT24, *Research in Snow, Ice and Frozen Ground,* Scientific Area A, *Properties of Cold Regions Materials,* Work Unit 004, *Properties of Cold Regions Hydrometeors.* The author thanks Harold W. O'Brien and Dr. Richard H. Munis of CRREL for their suggestions and technical reviews of this report.

This report describes a preliminary investigation of the extent and military applicability of present knowledge of ice fog as an electro-optical obscurant. Relationships are developed that may contribute to the Electro-Optical Systems Atmospheric Effects Library developed at the Atmospheric Sciences Laboratory, as well as providing initial guidelines (rules-of-thumb) for arctic sensor selection and utilization.

CONTENTS

ILLUSTRATIONS

ICE FOG AS AN ELECTRO-OPTICAL OBSCURANT

Gary Koh

INTRODUCTION

Ice fog is an atmospheric phenomenon visually resembling common water fog. However, ice fog usually occurs only when the ambient temperature drops below -30 °C, and generally increases in frequency, intensity and persistence with decreasing temperature. Under a microscope, the particles composing ice fog are seen to be minute ice crystals, approximately 2 to 20 μm in diameter.

During dense ice fog the visibility may be reduced to only a few meters. The optically degraded environment associated with ice fog generally occurs when water vapor resulting from combustion processes condenses on particulate matter to form small droplets that rapidly freeze into ice particles when introduced into a cold, stagnant air mass (Benson 1970). In inhabited areas, exhaust gases from home heating plants, factories, automobiles and aircraft are notorious contributors of raw materials for ice fog production.

The formation of ice fog with resultant low visibility can seriously restrict the effectiveness of military operations. A large-scale military operation conducted in arctic and subarctic regions with associated vehicular emissions, gunfire and other combustion activities is a potential source of the nucleating material and water vapor required for ice fog growth. With increasing dependence on electro-optical weapon systems, a model predicting the performance of electro-optical systems during ice fog is consequently of fundamental importance in the winter battlefield scenario. This necessitates a detailed knowledge of the processes of ice fog formation, the physical and optical properties of the ice fog, and an understanding of the electro-optical theory involved.

ICE FOG

Much of the research on the physical and optical properties of ice fog has been conducted at the Stanford Research Institute, the Geophysics Institute of the University of Alaska, and the U.S. Army Cold Regions Research and Engineering Laboratory. The properties of the ice fog discussed in this report were obtained from the extensive information provided by these organizations. The purpose of this review was to extract the basic concepts relevant to the study of ice fog as a cold regions obscurant.

Effects of atmospheric conditions on ice fog formation

The effects of battlefield activities on the formation of ice fog strongly depend on the nature of the activities and the ambient conditions. The ability to predict the impact of vehicular operation or gunfire in producing ice fog is of importance prior to tactical engagement. Therefore, the environmental conditions necessary for the formation of ice fog as a result of combustion activities should be identified.

A graph (Appleman 1953) of the temperature and humidity requirements for the formation of ice fog due to moisture produced by the burning of hydrocarbon fuels is reproduced in Figure 1. According to Appleman, ambient temperature and relative humidity will determine whether added moisture and heat from combustion will lower or raise the humidity of the affected environment. The critical temperature necessary for the humidity to increase from combustion activities as a function of initial humidity at 1000 mb is represented by curve AB. Thus ambient temperature

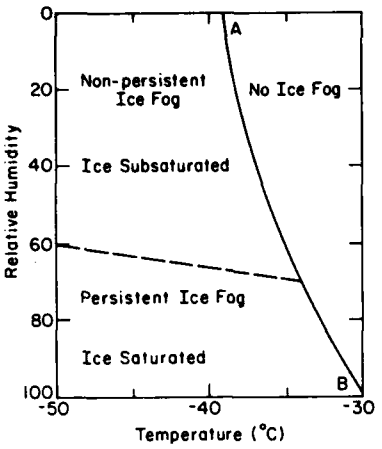

Figure 1. Temperature/humidity relationships for ice fog formation.

and humidity conditions must be in the region left of the curve for saturation to occur from added moisture from combustion. As an example, the initial humidity must exceed 50% for ice fog to occur from combustion activities at –35 °C, provided that enough moisture to produce saturation is released.

Warming-up and subsequent operation of aircraft or a large number of vehicles under the appropriate conditions will produce ice fog. The extent of the ice fog will depend on the amount of moisture present. The temperature and humidity regime where the condensation of droplets can occur may be either ice saturated or ice subsaturated (Fig. 1). If the vehicles are operating in an ice subsaturated environment, the dissipation of ice fog is likely, and one can expect localized plumes of ice particles around the vehicles emitting the exhaust. However, the introduction of moisture in an area near or at ice saturation can produce ice fog that may linger and whose duration will again depend upon the amount of moisture introduced by the battlefield activities and the rate of ice fog settling.

Ice fog is associated not only with vehicle operation but also with military activities. Kumai and O'Brien (1964) observed the effects of 155-mm howitzer activities in producing ice fog and reducing target visibility. The physical characteristics of the gunfire-generated ice fog were similar to those of ice fog generated from other sources. Camp activities of troops in a cold environment are an additional source of ice fog. The sources of ice fog are important to identify because the localized ice fog may be visible for many miles, with the potential of indicating the troops' presence.

The potential exists not only for predicting the formation of ice fog, but for determining its physical properties, given the nature of the water vapor source and the ambient conditions. The general theory of atmospheric ice crystal formation found in the literature of cloud physics can be applied to the growth of ice fog if the different environmental conditions associated with the two phenomena are taken into account. A theoretical study on the formation and growth of ice fog has been conducted by Huffman (1968). By applying the laws of thermodynamics and statistical mechanics, Huffman obtained the numerical values for the size distribution of ice fog in general agreement with his experimental results. A numerical model by Nelson (1972) for computing the size and concentation of ice fog particles produced by automobile exhaust again showed good agreement between the experimental and computed results. These models indicate that it may be possible to utilize a similar computer program to numerically characterize the ice fog resulting from battlefield activities.

An application of these numerical models is the determination of ways to reduce or enhance the transmission properties of the ice fog generated by vehicles. Nelson was able to affect the concentration and the size of the ice fog particles by varying some operating parameters of an automobile as inputs to his model. The size of the ice fog particles could be increased by increasing the exhaust pipe diameter or the exit temperature of the exhaust gas. Similar results can be achieved by decreasing the exit velocity of the exhaust gas or the concentration of soluble and insoluble particles in the exhaust. Given the dependence of the extinction properties of ice fog on the particle size/wavelength ratio and the size-dependent settling rate affecting the duration of the ice fog, further investigation into numerical modeling may be of interest.

Size distribution of ice fog particles

Knowledge of particle size distribution is required to calculate the attenuation of electromagnetic radiation transmitted through ice fog. For the parametric modeling of ice fog attenuation, the substitution of experimental size distribution data into an analytical expression is desirable. One analytical expression capable of realistically depicting the diverse shapes of the ice fog distribution is the modified gamma distribution used by Deirmendjian (1969) to model various atmospheric aerosols.

The modified gamma distribution is a three-parameter model expressed as

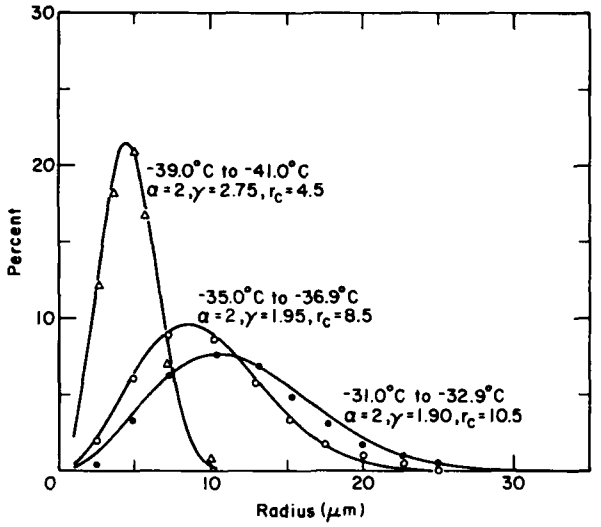

Figure 2. Modified gamma distribution for ice fog.

$$n(r) = ar^{\alpha} \exp[(-\alpha/\gamma)(r/r_c)^{\gamma}] \quad (1)$$

where $n(r)$ is a continuous and integrable function of radius r. The shape of the distribution is governed by α (positive integer), γ (positive constant) and r_c, which is the mode radius of the distribution. The value a normalizes the total number of particles in a unit volume and does not affect the shape of the distribution curve.

The temperature dependence of ice-fog crystal growth has been observed by various investigators. Thuman and Robinson (1954), Kumai (1964), Kumai and O'Brien (1964), and Ohtake (1970) employed impactors or electrostatic precipitators to collect and analyze ice fog crystals and noted the increase in the mean particle size with increasing temperature. The composite size distributions of ice fog occurring at temperatures of -31.0° to -32.9°C, -35.0° to -36.9°C and -39.0° to -41.0°C reported by Ohtake and the corresponding modified gamma distribution fit are illustrated in Figure 2. The modified gamma fit was approximated by trial and error because of the limited data set. Although the fit does not necessarily represent the optimum values, the versatility of the three-parameter model is demonstrated.

For future studies, optical measurement techniques can be used to obtain larger data sets of ice fog size distributions. This will necessitate a computational technique to obtain the best fit of the parameters to the measured data. Optimization programing, evaluating the deviation of the model distribution from the experimental data, is one potential method. This can be accomplished by minimizing a function of the form

$$F(\alpha,\gamma,r_c) = \sum_{i=1}^{m} [n_i - n(r_i)]^2 \quad (2)$$

where m is the number of experimental data pairs (n_i, r_i), and $n(r_i)$ is the modeled distribution.

Shape distribution of ice fog

An electromagnetic wave incident on a particle is scattered in all directions. The intensity of the scattered radiation measured at a given location is the resultant scattered radiation from the various parts of the scattering object. The phase differences of the scattered radiation become important when the size of the particle is comparable to or larger than the wavelength of the incident radiation. Comprehensive understanding of the scattering process requires not only this size factor to be considered but also the shape factor, since the phase relation of the scattered radiation, and thus the angular scattering pattern, are also dependent on the geometry of the scattering object.

The classification of ice fog particles according to shape conducted by previous investigators indicates that three general types of ice fog are present. Thuman and Robinson (1954) encountered mostly droxtals (near-spherical particles with rudimentary crystal faces) during ice fog occurring at temperatures below -38°C. However, with increasing temperature they observed that the per-

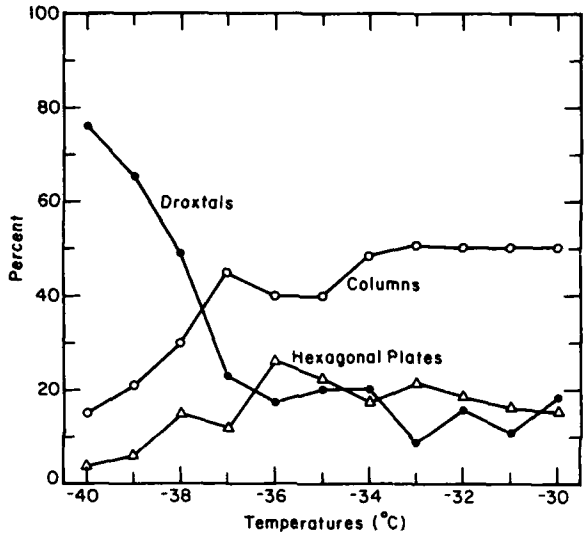

Figure 3. Shape distribution of ice fog.

centage of hexagonal plates and column-shaped crystals increased rapidly. Investigation of ice fog formed at temperatures below -37 °C (Kumai 1964, Kumai and O'Brien 1965) also indicated the prevalence of spherical particles with some plate-like and columnar structures. Ohtake's (1970) observations were consistent with those of previous investigators. He reported that hexagonal plates and columns accounted for over 60% of the ice fog crystals at temperatures above -37 °C. The temperature dependence of the shape distribution of ice fog (from the findings of Ohtake) is illustrated in Figure 3.

ELECTROMAGNETIC THEORY RELEVANT TO OPERATIONS IN ICE FOG

Electromagnetic radiation propagating through an ice fog medium is scattered and absorbed, thus incurring a path attenuation by a factor of $\exp[-B'_{ext}(\lambda)L]$. $B'_{ext}(\lambda)$ is the forward-scatter corrected extinction coefficient of the medium for wavelength λ, and L is the path length of the incident beam traversing the ice fog. This is the familiar Beer-Lambert relationship, and the term enclosed in the brackets represents the effective optical thickness of the medium. The extinction coefficient for a volume of air containing ice fog particles is determined by integrating the extinction properties of the individual particles of the volume and is expressed as

$$B_{ext} = \int_{r_{min}}^{r_{max}} \pi r^2 n(r)[Q_{sca}(m,x) + Q_{abs}(m,x)]\,dr \quad (3)$$

where πr^2 = geometrical cross-sectional area
$n(r)$ = size distribution function
Q_{sca}, Q_{abs} = efficiency factors for scattering and absorption
m = complex index of refraction of ice fog
x = size parameter, $2\pi r/\lambda$.

The scattering efficiency factor in this equation fails to take into account directional scattering, and thus neglects the forward-scattered component entering the field of view of the detector during transmittance measurements. Therefore, in order to compare the theoretical and experimental extinction coefficients, it becomes necessary to modify eq 3 to the following form:

$$B_{ext} = \int_{r_{min}}^{r_{max}} \pi r^2 n(r)[Q_{sca} - Q'_{sca} + Q_{abs}]\,dr \quad (4)$$

where Q'_{sca} is the efficiency factor associated with the scattered radiation entering the field of view of the detector and is determined from the angular scattering properties of ice fog and the geometry

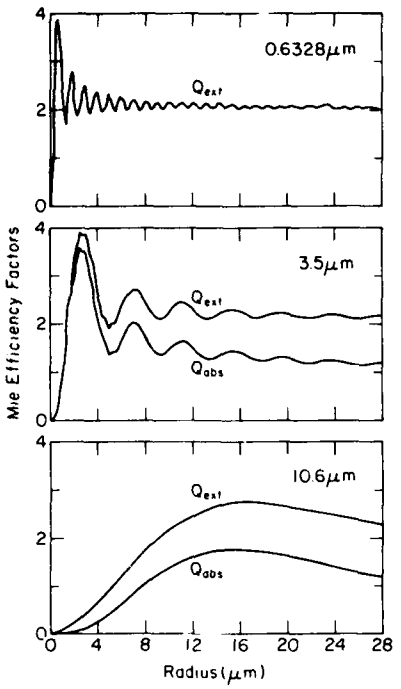

Figure 4. Mie efficiency factors for scattering and absorption.

of the transmission system. The multiple scattering effects are not considered in this report.

Because of the mathematical difficulties encountered in solving radiation scattering by randomly oriented asymmetrical particles, modeling of electromagnetic radiation through atmospheric aerosols generally assumes the sphericity of the particles. Rayleigh scattering and geometrical optics are the approximate solutions available for transmittance calculations through obscurants when the ratios of the particle size to the wavelength are very small and very large, respectively. When the wavelength of the incident radiation approaches the size of the interacting particles, the mostly widely employed solution technique is Mie theory, which is an exact solution to Maxwell's electromagnetic theory for a plane wave incident on a homogeneous sphere. Kumai and Russell (1969) and Seagraves (1981) applied Mie theory to determine the obscuring effects of ice fog for various wavelengths in the visible and infrared regions. Munis and Delaney (1972) and O'Brien and Kumai (1973) conducted transmission studies in laboratory-generated ice fog and found general agreement between the experimental extinction values and the values calculated using the Mie theory.

Application of Mie theory to ice fog

If the shape of the ice fog particles is assumed to be spherical, the scattering and absorption parameters of ice fog in the visible and infrared wavelengths can be derived from Mie theory. The detailed derivation of Mie theory can be found in the literature and is not repeated here. Only the commonly used parameters associated with Mie theory are defined here,and some thoughts on the applicability of Mie theory to the ice fog propagation model are presented.

The total energy scattered by a particle is derived by integrating the scattered energy over all scattering angles. The scattering cross-sectional area C_{sca} is then defined as the area that intersects as much radiation as is scattered by the particle. The expression of the energy scattered in terms of area permits normalization of the scattering parameter. The normalized scattering parameter commonly used is the scattering efficiency factor, which is the ratio of the scattering cross-sectional area to the geometrical cross-sectional area of the scattering particle. The Mie efficiency factors for extinction and absorption are normalized in the same manner. The efficiency factors

$$Q_{sca} = C_{sca}/\pi r^2, \quad Q_{abs} = C_{abs}/\pi r^2,$$

and $$Q_{ext} = C_{ext}/\pi r^2$$

for ice fog particles in the visible and infrared regions calculated using a computer program for Mie scattering, AGAUS 82 (Miller 1983), are shown in Figure 4. The complex index of refraction of ice used in the calculation is from Irvine and Pollack (1968).

The scattering cross-sectional area discussed previously does not contain information regarding angular scattering. The intensity distribution of scattered energy as a function of scattering angle is referred to as the phase function. This function is integrated over the detector's acceptance solid angle in order to correct for the forward-scattered energy that enters the field of view during transmittance measurement.

The applicability of Mie theory for use in an ice fog transmission model requires experimental data on the optical properties of ice fog to support the equivalent-sphere model presumed by Mie theory. Thuman et al. (1955), in an effort to determine the physical state of the suspended ice fog particles, measured the intensity of visible light scattered by ice fog in situ on 10 different occasions at

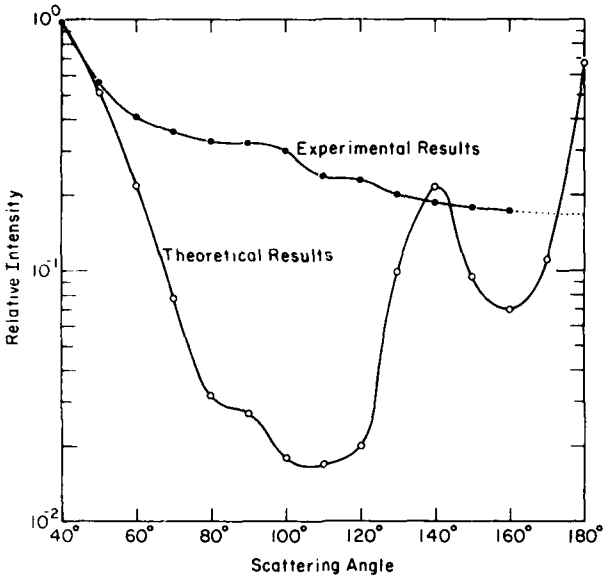

Figure 5. Comparison of experimental and calculated phase functions.

temperatures ranging from -34° to -40°C. The scattered intensity was measured in a horizontal plane at 10° intervals from 15 to 165°. Concurrent observation of the settled ice fog particles indicated that between 85% and 96% of the particles were of the droxtal type. (The large percentage of droxtals at the reported temperature range is not explained.) This large number of spherical particles provided a fortuitous opportunity for comparing the measured and calculated values of the angular variation of scattered light. An additional opportunity for comparative analysis was provided by Thuman with his scattering measurement conducted for ice fog composed of mostly prismatic columns and hexagonal plates. The ean radii reported for the ice fog composed of ly droxtals and the more developed crystals 6.0 and 6.5 μm, respectively.

AGAUS 82 computer program for Mie ring (Miller 1983) was utilized to obtain the eoretical scattering pattern for an ensemble of e spheres with similar size distribution to the ice og encountered by Thuman. Comparison of the measured and calculated values normalized to coincide at 40° is shown in Figure 5. The presence of a minimum and a maximum at the respective lateral and backscatter angles in the theoretical values does not occur with the experimental results. Rather, the shape of the experimental values for the angular variation of scatter radiation departs from the equivalent sphere model and more closely resembles scattering patterns observed for irregular particles. An important observation not shown in Figure 5 was that no significant differences were apparent in the light-scattering properties of the droxtal types and the more developed ice fog crystals. This implies that the same phase function can be used to describe the scattering properties of the different types of ice fog in the visible region.

The limited data available for the radiation scattering properties of ice fog necessitate more definitive experiments in the future. Until these measurements are available, phase function measurements conducted for artificially generated ice crystals can be evaluated for analogous results. Laboratory measurements of the phase function of laboratory-generated ice particles provide a realistic representation of an in-situ ice fog. These measurements (Huffman and Thursby 1970 and Sasson and Liou 1978) again indicated greater side scattering by ice crystals than indicated by the computed results for spherical assemblies. Given the experimental evidence accumulated thus far, one can conclude that Mie theory can be applied for forward-scattering problems in ice fog, but limitations exist for side and backscatter calculations.

In-situ measurements of infrared radiation scattering by ice fog do not appear in the literature. However, laboratory measurements of infrared (10.6 μm) scattering by artificially generated ice

crystals of plate and columnar structure provide valuable insight into the potential scattering properties of ice fog in the infrared region (Sasson 1981). The angular scattering pattern produced by the ice crystals again deviates from Mie values employing the equivalent-sphere model. As in the visible regions where the near-forward scattering efficiency can be determined from Mie theory, forward-scattering by ice fog in the infrared regions may also be determined in this manner.

The experimental data available appear to indicate that the utility of Mie theory for an ice fog propagation model in the visible and infrared regions of the spectrum is limited to forward scattering. Applications requiring knowledge of the scattering properties of ice fog in all directions will require modeling of the scattering process employing judicious use of empirical and theoretical results.

Comparisons of infrared to visible volume extinction coefficients

Comparison of the transmission properties of various wavelengths through an obscuring medium can serve as a guideline in selecting the electro-optical system capable of optimal performance through the given medium. With this in mind, the relationship between the visible and infrared extinctions through ice fog is investigated. The influence of ice fog particle size on extinction properties in the visible and infrared regions has been previously illustrated (Fig. 4). Given this fact, one can conclude that the shape of the ice fog size distribution curve will have a significant role in influencing the infrared to visible extinction ratios. In an effort to determine the effect of the size distribution in this relationship, comparative extinction values were calculated for a broad range of ice fog distributions expressed in terms of the modified gamma distribution.

The solution for determining the extinction coefficient through an ice fog medium represented by the modified gamma distribution is derived from eq 1 and 3. Forward-scattering corrections (eq 4) are not considered in the following calculations since the transmission geometry can vary depending on the electro-optical system in use. Integration of eq 1 (Dwight 1961) over the entire range of radii yields the total number of particles N per unit volume where

$$N = (a/\gamma)\left(\frac{\alpha}{\gamma r_c^{\gamma}}\right)^{-(\alpha+1)/\gamma}\Gamma\left(\frac{\alpha+1}{\gamma}\right). \quad (5)$$

Rearranging this equation for a,

$$a = \frac{N\gamma}{\Gamma\left(\frac{\alpha+1}{\gamma}\right)}\left(\frac{\alpha}{\gamma r_c^{\gamma}}\right)^{(\alpha+1)/\gamma} \quad (6)$$

indicates that the value for a is determined by N. The extinction coefficient for an ice fog distribution, given the number concentration, can now be expressed as

$$B_{ext} = \frac{N\gamma}{\Gamma\left(\frac{\alpha+1}{\gamma}\right)}\left(\frac{\alpha}{\gamma r_c^{\gamma}}\right)^{(\alpha+1)/\gamma} \times \int_{r_{min}}^{r_{max}} \pi r^2 Q_{ext} r^{\alpha} \exp[(-\alpha/\gamma)(r/r_c)^{\gamma}]\,dr. \quad (7)$$

The volume extinction coefficients were calculated for 0.6328-μm, 3.5-μm and 10.6-μm regions. The size distribution parameters were chosen to encompass a broad range of distribution shapes in order to identify the influence of size distribution on the extinction properties at the selected wavelengths. The relative extinction properties were evaluated for 115 different distributions represented by the following combinations of parameters:

$\alpha = 2.0$

$\gamma = 0.75, 1.0, 1,5, 1.95, 2.75$

$r_c = 1.0$–12.0 μm at 0.5-μm intervals.

These combinations of parameters do not necessarily represent actual experimental ice fog distribution data. They are presented for continuity to demonstrate the sensitivity of the infrared to visible extinction ratios to the modified gamma parameters. However, the distributions for ice fog occurring at different temperature ranges reported by Ohtake (1970) have been included in this investigation. One can also assume that many of the distributions are in fact realistic representations of ice fog distributions.

The relative performance of the 3.5-μm wavelength with respect to the visible radiation is not favorable (Fig. 6). Although the transmission at 3.5 μm improves with increasing particle size distribution, the visible radiation is less obscured

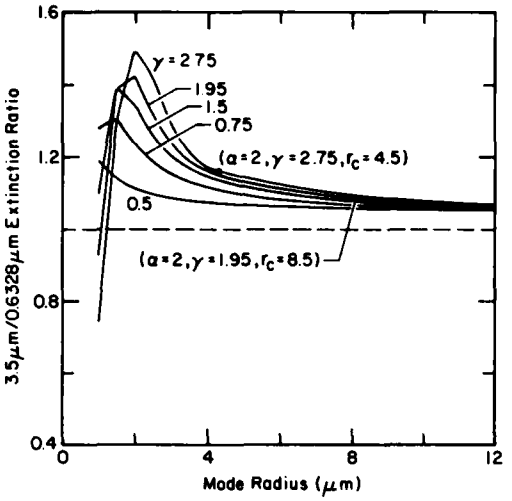

Figure 6. 3.5-μm/0.6328-μm extinction ratio.

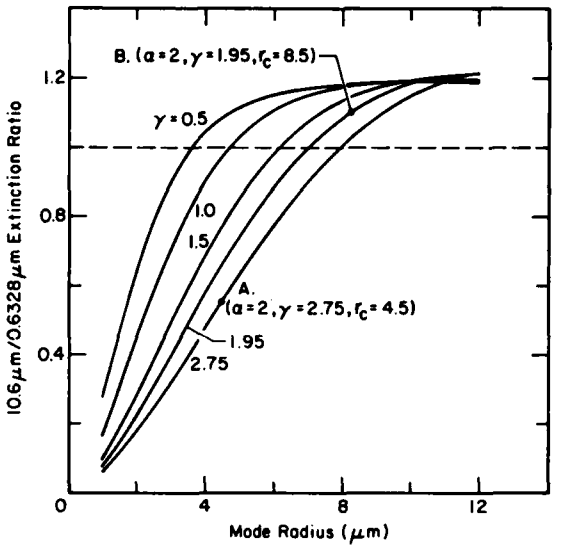

Figure 7. 10.6-μm/0.6328-μm extinction ratio.

than that at 3.5 μm for all distributions likely to be encountered in ice fog. The comparison of 10.6 μm to visible radiation is perhaps more interesting, due to the crossover in the relative performances of the two wavelengths (Fig. 7). The 10.6-μm wavelength, relative to the visible, degrades noticeably with increasing size distributions, indicating that with increasing temperature one can expect visible systems to outperform infrared systems. Specifically, the extinction ratio of the 10.6 μm to 0.6328 μm in ice fog formed at temperatures below -38 °C (e.g. A, representing the composite ice fog size distribution formed around -39° to -41 °C as reported by Ohtake) is approximately 0.55, yet actually exceeds unity for ice fog size distributions associated with increasing temperatures (e.g. B, showing ice fog typical of that formed around -35° to -36.9 °C).

10.6-μm extinction as a function of ice fog mass concentration

The volume extinction coefficient for the 10.6-μm wavelength can, within limits, be approximated as a function of the ice fog mass concentration (*MC*) pseudo-independently of the ice fog distribution. This relationship assumes that the maximum radius of the ice fog particles in any given distribution is around 12.0 μm, or, if larger particles exist, that they do not contribute significantly to either the B_{ext} or the *MC*. The *MC* is often a more easily obtainable parameter than the size distribution. Therefore the utility of this relatively simple relationship can be incorporated into the ice fog propagation model. The procedure for identifying a specific wavelength whose extinction coefficient is a function of *MC* was outlined by Chýlek (1978) for fog and cloud droplets.

The *MC* of ice fog is expressed as

$$MC = \frac{4\varrho_i}{3} \int_{r_{min}}^{r_{max}} \pi r^3 \, n(r) \, dr \qquad (8)$$

where ϱ_i(0.91 g/cm³) is the density of ice. The volume extinction coefficient is related to the *MC* in the following form:

$$B_{ext} = \frac{3}{4} \frac{MC}{\varrho_i} \frac{\int_{r_{min}}^{r_{max}} \pi r^2 \, n(r) \, Q_{ext} \, dr}{\int_{r_{min}}^{r_{max}} \pi r^3 \, n(r) \, dr} \qquad (9)$$

The extinction efficiency factor Q_{ext} for the 10.6-μm wavelength can be approximated by a linear relationship (Fig. 8), such that

$$Q_{ext} = 0.21 \, r \qquad (10)$$

where the maximum radius is around 12.0 μm. Substituting this new value for Q_{ext} into eq 9 yields

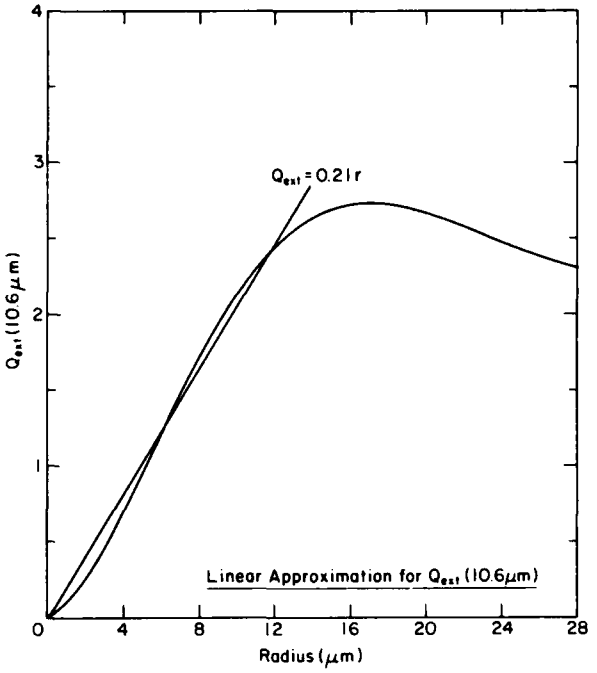

Figure 8. Linear approximation for Q_{ext}.

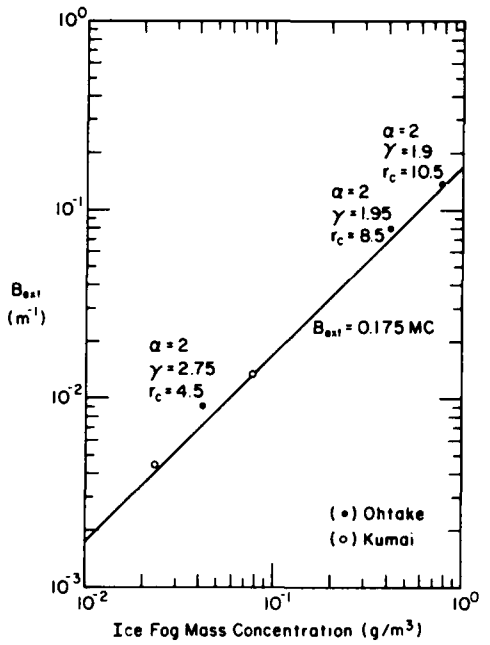

Figure 9. 10.6-μm extinction as a function of ice fog mass concentration.

$$B_{ext} = (0.21)\ \frac{3}{4}\ \frac{MC}{\varrho_i}\ \frac{\int_{r_{min}}^{r_{max}} \pi r^3\, n(r)\, dr}{\int_{r_{min}}^{r_{max}} \pi r^3\, n(r)\, dr} \qquad (11)$$

Finally, canceling of the integral on the right side of the equation results in a size-distribution-independent relationship between the 10.6-μm extinction and the *MC* of ice fog, which is simply

$$B_{ext} = 0.17\, MC. \qquad (12)$$

In order to evaluate how accurately the *MC*-dependent extinction values approximate the exact solution, comparative results were analyzed. The composite size distributions for the three temperature ranges reported by Ohtake (Fig. 2) were evaluated. The *MC* values of the three distributions for the arbitrarily selected number density of 100 particles/cm³ were derived by multiplying $n(r)$ in eq 1 by $^4/_3 \pi r^3 \varrho_i$ and integrating to yield

$$MC = {}^4/_3 \pi a\ \frac{\varrho_i}{\gamma}\left(\frac{\alpha}{\gamma r_c^\gamma}\right)^{-(\alpha+4)/\gamma} \Gamma\left(\frac{\alpha+4}{\gamma}\right) \qquad (13)$$

Substituting the value a in eq 6 gives

$$MC = {}^4/_3 \pi \varrho_i N \left(\frac{\alpha}{\gamma r_c^\gamma}\right)^{-3/\gamma} \frac{\Gamma[(\alpha+4)/\gamma]}{\Gamma[(\alpha+1)/\gamma]} \qquad (14)$$

Then, using the approximate relationship (eq 12) the volume extinction coefficients were calculated. Also, the extinction coefficients were calculated using the exact solution (eq 7) for identical number density. The comparative results are shown in Figure 9. The line represents the extinction coefficient as a function of the ice fog mass concentration independent of the size distribution. The result seems to indicate that, given only the *MC* of ice fog, the 10.6-μm extinction coefficient can be approximated within reasonable accuracy. Additional verification of the *MC* to 10.6-μm extinction relationship is demonstrated by similar comparative analyses of size and mass distributions of ice fog (also shown in Fig. 9) reported by Kumai (1964).

CONCLUSIONS

Ice fog can present serious visibility/electro-optical system performance problems during military operations in arctic and subarctic regions.

Thus, knowledge of the physical and optical properties of ice fog is necessary to predict the performance of electro-optical systems in this environment. It appears that the potential exists not only for predicting the formation of ice fog, but also for determining its physical properties, given the nature of the water vapor source and the ambient conditions.

Based on experimental evidence to date, it may be concluded that Mie theory can be applied to determine forward-scattering properties of ice fog in the visible and infrared wavelengths, but that limitations exist for applications involving significant side and backscatter.

Visible radiation is somewhat less subject to obscuration by ice fog than is infrared radiation of 3.5-μm wavelength, regardless of temperature. However, the extinction of 10.6-μm radiation relative to that of visible radiation is dependent on the size distribution of the ice fog, which is in turn temperature-related. It appears that ice fog is considerably more transparent to 10.6-μm radiation than to visible radiation at temperatures below about -38°C, whereas at higher temperatures the reverse is likely to be true.

On the basis of some reasonable assumptions concerning the probable lack of contribution to obscuration by large ice particles in ice fog, it has been shown that the volume extinction coefficient at 10.6 μm may be represented as being directly proportional to the mass concentration of ice fog particles in the air. The proportionality constant is shown to be 0.17 *MC*.

LITERATURE CITED

Appleman, H. (1953) The cause and forecasting of ice fogs. *Bulletin, American Meteorological Society,* **34**(9): 397-399.

Benson, C.S. (1970) Ice fog: Low temperature air pollution. USA Cold Regions Research and Engineering Laboratory, CRREL Research Report 121. AD 708544.

Chýlek, P. (1978) Extinction and liquid water content of fogs. *Journal of Atmospheric Sciences,* **35**: 296-300.

Deirmendjian, D. (1969) *Electromagnetic Scattering on Spherical Polydispersions.* New York: Elsevier.

Dwight, H.B. (1961) *Tables of Integrals and Other Mathematical Data.* New York: MacMillan.

Huffman, P.J. (1968) Size distribution of ice fog particles. Masters Thesis, University of Alaska (unpublished).

Huffman, P.J. and W.R. Thursby (1969) Light scattering by ice crystals. *Journal of Atmospheric Sciences,* **26**: 1073-1077.

Irvine, W.M. and J.B. Pollack (1968) Infrared optical properties of water and ice spheres. *Icarus,* **8**: 324-360.

Kumai, M. (1964) A study of ice fog and ice-fog nuclei at Fairbanks, Alaska. USA Cold Regions Research and Engineering Laboratory, CRREL Research Report 150, Part I. AD 451667.

Kumai, M. and H.W. O'Brien (1965) A study of ice fog and ice-fog nuclei at Fairbanks, Alaska. USA Cold Regions Research and Engineering Laboratory, CRREL Research Report 150, Part II. AD 451667.

Kumai, M. and H.W. O'Brien (1964) Ice fog formation by 155-mm howitzer. USA Cold Regions Research and Engineering Laboratory, CRREL Technical Note (unpublished).

Kumai, M. and J.D. Russell (1969) The attenuation and backscattering at infrared radiation by ice fog and water fog. USA Cold Regions Research and Engineering Laboratory, CRREL Research Report 264. AD 689447.

Munis, R.A. and A.J. Delaney (1972) Measurement of laser extinction in ice fog for design of SEV pilotage system. USA Cold Regions Research and Engineering Laboratory, CRREL Research Report 302. AD 750114.

Miller, A. (1983) Mie code AGAUS 82. U.S. Army Atmospheric Sciences Laboratory. ASL-CR-83-0100-3.

Nelson, W. (1973) Computation of the size and concentration of ice particles produced by auto exhaust in arctic climates. *The Northern Engineer,* **5**(3): 10-12.

O'Brien, H.W. and M. Kumai (1973) Transmission of 2.0 to 3.4 micron infrared radiation in ice fog. USA Cold Regions Research and Engineering Laboratory, CRREL Special Report 189. AD 657 580.

Ohtake, T. (1970) Studies on ice fog. University of Alaska Geophysical Institute, Report UAGR-211.

Sasson, K. (1981) Infrared (10.6 μm) scattering and extinction in laboratory water and ice clouds. *Applied Optics,* **20**(2): 185-193.

Sasson, K. and K.N. Liou (1979) Scattering of polarized laser light by water droplets, mixed phase and ice crystal clouds. Part 1: Angular scattering

patterns. *Journal of Atmospheric Sciences,* **36:** 838-851.

Seagraves, M.A. 1981) Visible and infrared obscuration effects of ice fog. U.S. Army Atmospheric Science Laboratory. ASL-7R-0084.

Thuman, W.C. and E. Robinson (1954) Study of Alaskan ice fog particles. *Journal of Meteorology,* **11:** 151-156.

Thuman, W.C., G.A. St. John, and I.G. Poppoff (1955) Studies of the intensity of light scattered by water fogs and ice aerosols. Stanford Research Institute Scientific Report V.

A facsimile catalog card in Library of Congress MARC format is reproduced below.

Koh, Gary
Ice fog as an electro-optical obscurant / by Gary Koh.
Hanover, N.H.: Cold Regions Research and Engineering Laboratory; Springfield, Va.: available from National Technical Information Service, 1985.
iv, 18 p., illus., 28 cm. (CRREL Report 85-8.)
Prepared for Office of the Chief of Engineers, by Corps of Engineers, U.S. Army Cold Regions Research and Engineering Laboratory under DA Project 4A161102AT24.
Bibliography: p. 10.
1. Electromagnetic radiation. 2. Ice fog. 3. Obscuration. I. United States. Army. Corps of Engineers. II. Cold Regions Research and Engineering Laboratory, Hanover, N.H. III. Series: CRREL Report 85-8.